Renewable Energy 237 (2024) 121601

Contents lists available at ScienceDirect

Renewable Energy

journal homepage: www.elsevier.com/locate/renene

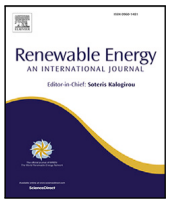

Assessing hydrodynamic impacts of tidal range energy impoundments in UK coastal waters

Edward Roome [a,*], Peter Robins [a], Reza Ahmadian [b], Martin Austin [a], Nicolas Hanousek [b], Bin Guo [c], Simon Neill [a]

[a] Bangor University, School of Ocean Sciences, Menai Bridge, LL59 5AB, UK
[b] Cardiff University, School of Engineering, Cardiff, CF24 3AA, UK
[c] National Oceanography Centre, Joseph Proudman Building, Liverpool, L3 5DA, UK

ARTICLE INFO

Keywords:
Tidal range schemes
Tidal lagoon
Tidal dynamics
Marine renewable energy
Ocean modelling

ABSTRACT

Tidal range energy comprises a vast theoretical resource of 9,220 TWh per year, globally, with advantageous characteristics of predictability, generation flexibility and reliability. Approximately 13% of this resource lies within the United Kingdom's (UK) coastal waters, where it could supply up to 12% of annual electricity demand. Tidal range energy conversion traditionally involves constructing and operating large-scale coastal or offshore impoundments ($\mathcal{O}$10-100 km^2), which will redefine near and far-field water levels and flow patterns. The relationship between the scale of the impoundment area and hydrodynamic impact has not been investigated for UK sites. To address this, we develop a two-dimensional (depth-averaged) TELEMAC model of the Irish Sea, and simulate six scenarios involving tidal range schemes of increasing basin area, from 25 to 150 km^2, located on the North Wales coast in an open coastal basin setting. Results indicate that far-field (30 – 150 km) changes to the amplitude of the semi-diurnal (M_2) tidal constituent exhibit a linear relationship with impoundment area and volume (correlation coefficient $R = 0.95$ and $R = 0.96$, respectively). The largest impoundment (150 km^2) caused far-field changes in maximum surface elevation ($2 < \eta_{max} < 3$ cm); near-field surface elevation was reduced ($\eta_{max} > 3$ cm).

1. Introduction

The world faces an energy trilemma — ensuring a secure supply of affordable electricity amid rising demand [1] and geopolitical uncertainty, whilst mitigating anthropogenic climate change by implementing a low-carbon emission future [2]. Under international treaty, many nations have agreed to decarbonise their energy systems; if executed successfully, this will involve exploiting diverse sources of renewable energy [3,4]. Amongst these, tidal range energy offers some nations, including the UK, France, Canada, Australia and Argentina, a vast and untapped resource (9220 TWh [5], globally[1]) that is variable over tidal and lunar cycles but, importantly, predictable for decades into the future [6]. Globally, around 520 MW of ocean renewable energy is currently installed, of which tidal range contributes 500 MW [6], considerably larger than tidal stream which stands at 10 MW [7].

In regions of large tidal range (mean > 5 m, [8]), a tidal range scheme (TRS) is deemed viable and can harness the potential energy stored within the vertical movement of the tide. The plant operates by creating an artificial water level difference between an impounded water body and the open water. Gravity-driven flow through hydroelectric (uni- or bi-directional) turbines generates electricity and Sluice gates are used to manage basin water levels and required flow conditions. Globally, there are four operational TRSs [6],[2] each uses a *barrage* type impoundment perimeter which stretches across an estuary. Alternatively the impoundment can extend along a coastline, or be located entirely offshore; these concepts are referred to as *coastal* or *offshore* tidal lagoons, respectively [9]. No operational tidal lagoons exist, but they are popular amongst recent TRS proposals, despite their higher (levelised) cost relative to tidal barrages [10]. Because tidal lagoons can be positioned to occupy less valuable ecological space and do not have to block fish migration entirely by blocking the estuary, they are therefore considered to cause less environmental disruption, relative to tidal barrages [11] — this has been a driving factor behind the recent interest in tidal lagoon research.

* Corresponding author.
E-mail address: e.roome@bangor.ac.uk (E. Roome).

[1] The majority of the tidal range resource is distributed among eleven countries. Note that the global theoretical resource (9220 TWh) excludes the Hudson Bay which is unsuitable for tidal range energy conversion (due to extensive sea ice).

[2] The Annapolis Royal Tidal Power Station was closed in 2019.

https://doi.org/10.1016/j.renene.2024.121601
Received 25 June 2024; Received in revised form 4 October 2024; Accepted 10 October 2024
Available online 18 October 2024

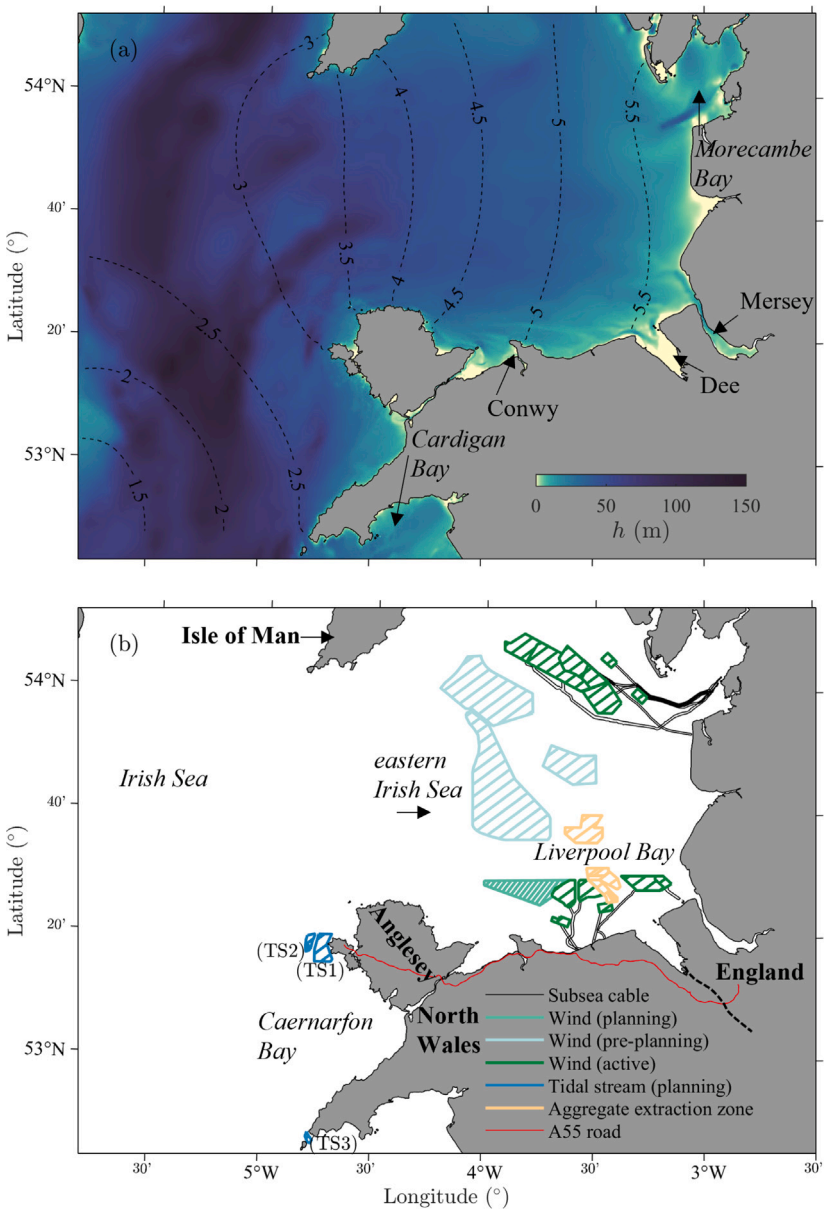

Fig. 1. Study region. (a) Nearshore water depth (h, presented on a non-linear scale) relative to MSL, black dashed contours show the mean tidal range, calculated from $2 \times \alpha_{M2}$ (where α is amplitude). (b) Key infrastructure in the region of North Wales, labels TS1, TS2 and TS3 show the West Anglesey, Holyhead Deep, and Bardsey Sound tidal stream sites, respectively (see Table 5). Pertinent islands (bold), maritime regions (italics) and estuaries are labelled in (a) and (b).

Off Britain's west coast, the Bristol Channel/Severn Estuary and eastern Irish Sea experience large tidal ranges — the Severn Estuary has a maximum tidal range in excess of 14 m, the second largest globally [6]. Hence, the UK's shelf seas harbour 13% (734 TWh) of the global theoretical tidal range resource [6]. The development of various TRSs has been considered over the past 100 years, particularly in the Severn Estuary [12]. Climate change targets require the UK's carbon-free electricity production capacity to increase from 42% (in 2022) to 100% by 2035 [13], therefore TRS proposals have received a renewed surge of attention from industry [14], academia and government [15,16]. It is estimated that, a fleet of TRSs could supply 10% of the UK's annual electricity demand (based on 22 GW of installed capacity supplying 33 TWh per year, see Ref. [17]). However, despite the general success of tidal range projects abroad (e.g. the La Rance Tidal Power Station in France was commissioned in 1966 [18]), the UK is yet to deploy any form of TRS.

A viable (modest) sized tidal lagoon will impound an area of around 10 km^2 and contain 1.5 km^3 of seawater (assuming an average depth of 15 m). Due to the periodic diversion of such large volumes of water, tidal lagoons will redefine local and far-field water levels, flow patterns, and morphodynamics [19–21]. As a large-scale coastal structure, a TRS substantially modifies the coastline, this impedes on macro-tidal processes, resulting in far-reaching impacts on tidal amplitudes and sea surface variability from waves and surges. Uncertainty around the magnitude and extent of these hydro-environmental impacts remains one of the main barriers to developing a tidal lagoon project [22].

Hydrodynamic modelling can be used to assess and optimise TRS design parameters to limit hydro-environmental impacts (e.g., [23]) and to improve the maximum, or the distribution of, electricity generation and use (e.g., [24,25]). Researchers have investigated the hydro-environmental response to changes in the shape, size [23], location [20], operational mode [11] and turbine/sluice arrangement of TRSs [26]. However, the unique nature of coastal systems makes the generic application of these results difficult [27]. Assessments of individual TRSs are required to optimise parameters and ascertain hydro-environmental impacts prior to construction.

To the authors knowledge, the relationship between impoundment size and hydrodynamic impact is yet to be characterised for a tidal lagoon in UK coastal waters (although [23] conducted a similar study for TRSs located in the Bay of Fundy, Canada). Thus, we investigate the impact of impoundment surface area A_s (at mean sea level; MSL) by modelling six tidal lagoon designs (where A_s ranges from 25–150 km^2, see Fig. 4 and Table 1); each tidal lagoon is a scale-variation of the design proposed by North Wales Tidal Energy [14].

This study addresses the following research gaps:

1. Understanding the sensitivity of mesoscale (10–100 km) hydrodynamic response to tidal lagoon impoundment size.
2. Expanding on (1), we examine the impacts of the tidal lagoons on the amplitude of the principle tidal harmonics and their relationship to the tidal lagoon characteristics across far-field and near-field regions.
3. Expanding on (1), we examine the nature of the relationship between impoundment size and hydrodynamic impact (current velocities and bed shear stress) for each scenario.

2. North Wales tidal lagoon: site characterisation

The North Wales coast is an attractive tidal lagoon site for the following reasons: the region experiences a high tidal range[3] (Fig. 1), deep waters are found adjacent to shallow regions — favourable for siting hydro-electric turbines and cost-effective embankment construction[4] [14], opportunities for local grid connection and hybridisation of power generation with offshore wind (Fig. 1), and the potential to reduce coastal flood risk for some low-lying regions[5] [29]. The Colwyn Bay Tidal Lagoon, proposed by North Wales Tidal Energy [14], is the only publicly-available industry-proposed current tidal lagoon proposal along the coast of North Wales. However, academics have conducted hydro-environmental assessments for hypothetical tidal lagoon designs which have not been proposed by industry [20].

Along the North Wales coast, tidal conditions strongly influence shoreline stability, the risk of coastal flooding, biogeochemical pathways, pollution dispersal and sediment transport [30]. Tidal conditions (currents and water levels) support a variety of pelagic and benthic habitats. From turbid water columns and bedrock outcrops in the region of the Anglesey turbidity maxima [31], to relatively quiescent regions in which vast mudflats have developed, or subtidal sandbanks (e.g. Constable Bank, described in detail by [30] and shown in Fig. 11). Turbidity maximas – regions of high suspended sediment concentrations – are nutrient dense, productive, regions which hold economical importance as nursery areas for marine species [32]. The sensitivity of current speeds in these environments in relation to tidal lagoon size is yet to be assessed for the North Wales region.

The eastern Irish Sea is a relatively shallow region, with a mean water depth of 30 m and several estuaries (which contribute 70% of the total riverine input; [33]). The Liverpool Bay region (eastern Irish Sea) receives the highest freshwater input (233 $m^3\ s^{-1}$). Baroclinic effects (such as tidal straining) can extend along the North Wales coast, during neap tides the freshwater plume can extend to 4°W [34]. In the region north of Constable Bank, located in Fig. 11a, the magnitude of these baroclinic currents have been estimated: 4 $cm\ s^{-1}$ (surface) and 2.4 $cm\ s^{-1}$ (near the bed; see Refs. [34,35]) — an order of magnitude smaller than those generated by the astronomical tides [30]. The tidal wave, which is dominated by the M_2 and S_2 constituents, propagates northwards into the Irish Sea from the Celtic Sea; peak tidal current speeds can exceed 2 $m\ s^{-1}$ during spring tides around headlands and through straits (e.g. NW coast of Anglesey and Menai Strait [36,37]). Because of the decreased propagation speed c of the tidal wave in shallow water ($c = \sqrt{gh}$), the distance from the Celtic Sea to Liverpool Bay and the wavelength of the semi-diurnal tide — the M_2 harmonic is in near-resonance in the northeast Irish Sea. Therefore, large M_2 amplitudes are observed across the region (e.g. Mersey and Solway Firth; Fig. 1). In the eastern Irish Sea, the reduced water depth induces strong non-linear effects due to tidal friction, which generates the M_4 harmonic. When combined with M_2, a flood dominant tidal regime arises [38,39]; the shorter-duration flood phase exhibits current velocities 1.2 times greater than the longer ebb phase [40]. The North Wales coastline is generally sheltered from swell waves (generated in the Atlantic and propagating through the Celtic Sea), however the coastline is exposed to infrequent (localised) wind wave events from the north [41]. In the eastern Irish Sea, the seabed mostly consists of sandy sediments of glacial origin, ranging from fine to coarse, these sediments are arranged into various bedforms (e.g. offshore sandbanks; [42,43]). Mean grain size in this region is strongly correlated with tidal-induced bed shear stress and peak current speed, therefore sediment transport and bed morphology is highly sensitive to tidal conditions [44,45].

Across the region, the activities of various economically important industries (e.g. aquaculture, fisheries and marine energy, Fig. 1b), populated areas (e.g. Colwyn Bay, Llandudno and Liverpool) and infrastructure (e.g. coastal rail and road transport links) are sensitive to changes in tidal conditions. Low coastal relief and a rate of erosion of 10–20 mm per year (due to a net eastward drift of sediment; [30]) increases the risk of coastal flooding (evident in the extensive history of flood events from Colwyn Bay to Rhos-on-Sea; [29]). Furthermore, the latest report from the Intergovernmental Panel on Climate Change (IPCC) advises that sea levels may rise between 28 and 101 cm by 2100 [46]. Sea-level rise and changes in extreme weather events (magnitude and frequency) are predicted to exacerbate compound flooding events [47,48]. Indirect, non-linear effects of an increased MSL also include the reduced capacity for artificial and natural defences (e.g. seawalls or sandbanks) to diffuse wave energy [49]. By altering the present tidal conditions, a tidal lagoon could have a significant impact on beach stability, coastal ecology and flooding. Minimising these impacts whilst maximising electricity generation is fundamental to the success of tidal range energy projects [6].

3. Methodology

3.1. TELEMAC modelling system

In this study, we applied the open source TELEMAC 8.2 model [50]. TELEMAC[6] operates on an unstructured fine-element grid, suitable for resolving undulating coastlines and intertidal regions. TELEMAC-2D is the depth-averaged hydrodynamics module used in this study (this is consistent with previous TRS simulations e.g. Refs. [21,23,51]). TELEMAC-2D solves the Saint-Venant equations of momentum and continuity (see Ref. [50]). Since the model is depth-averaged, we assumed barotropic flow (these are orders of magnitude larger than the baroclinic currents, see Section 2) and there is a need to parameterise internal friction. To simulate turbulence, we used the $k-\epsilon$ turbulence model with a conjugate residual solver — Guo et al. [52] showed that the $k-\epsilon$ model is the most accurate approach for resolving tidal flows around coastal structures (i.e. tidal lagoons). After testing the accuracy of the bed friction methods available in TELEMAC-2D, Manning's Law was the selected parameterisation method (Eq. (5); [50]), subsequent calibration involved tuning the spatially uniform friction coefficient n (in units of $s\ m^{-\frac{1}{3}}$) – a value of 0.03 was optimal (results shown in Supplementary Table S1). Intertidal regions are handled by a wetting

[3] At Llandudno, the average neap and spring tidal range is 3.77 m and 7.20 m, respectively [28].

[4] Due to the high costs associated with building an embankment in water depths > 25 m [6].

[5] However, these findings are highly dependent on the modelling approach.

[6] http://www.opentelemac.org/.

and drying algorithm (further described by [53]); the minimum depth is set to 0.05 m. Spatial discretisation involved applying the quasi-bubble triangle to solve the velocity field and the linear triangle to solve surface elevations [54].

3.1.1. Application to the Irish Sea

The computational domain covers the Irish Sea and extends to the edge of the continental shelf where water depths exceed 300 m (Fig. 2a). An unstructured mesh of triangular elements, generated in BlueKenue [55], was used to spatially discretise the computational domain (Fig. 2b). The grid spacing is decreased from 300 m in the centre of the tidal lagoon to 30 m at the embankment (the lagoon designs are described in the next subsection), grid spacing ranges from 1000 m to 30 m along coastlines (depending on proximity to lagoon) and increases to 3000 m in the middle of the Irish Sea and 6000 m along each open boundary.

Model bathymetry represents a compilation of multiple datasets, each reduced to MSL and linearly interpolated onto the mesh. Across the wider domain, the EMODnet 2022 bathymetric data were used (at 115 m resolution[7]). In the North Wales region, a combination of data sources have been utilised: (1) intertidal LiDAR data (at 2 m resolution[8]), (2) multibeam echosounder (MBES) data collected by Bangor University (available at <5 m resolution covering various coastal regions[9]), and (3) Admiralty chart data for offshore regions of the eastern Irish Sea.[10]

When simulating a TRS, open boundaries in the numerical model must be located sufficiently far from the structure so that the forcing conditions (calculated in global tidal models e.g. OTIS [56] – without the inclusion of a TRS) are not significantly affected by the operation of a TRS. Secondly, the physical structure and operating procedures of a TRS can induce small changes in shelf resonance (caused by the sudden increase in depth; [57]). To satisfy these criteria, the open boundaries must cover the shelf edge regions [20,58].

Two open boundaries; located in the SW Celtic Sea and NW Atlantic are featured in the model domain (as shown in Fig. 2a). At each open boundary, the model is forced with 22 tidal constituents from TPXO9.v5a database (which has an average RMSE of <5 cm in the open ocean — data is provided at 1/6° resolution; [56]). The TPXO9.v5a database includes the five principle semi-diurnal (M_2, S_2 and N_2) and diurnal (K_1 and O_1) constituents, which explain 90.5% of sea-level variation in our study region (co-tidal charts are given in Supplementary Fig. S1). As discussed in Section 2, the magnitude of freshwater driven currents are relatively small [59], and since the focus is on meso-scale tidal dynamics, and because the model is 2D (and will not simulate stratification), we neglect freshwater input in the model.

The model has been configured to run in parallel mode on high performance computers (Supercomputing Wales[11]). The simulation period was 30 days from 2018/04/01 00:00:00, chosen to coincide with an ADCP deployment (the diamond marker in Fig. 2b shows the deployment location). Following a sensitivity analysis, we selected a constant time step Δt = 5 s to ensure numerical stability. A 3-day spin-up period was implemented to allow the model to stabilise before the outputs were saved. Due to the size of the model domain, the WGS84 geographic coordinate system was used; this allows TELEMAC to vary the Coriolis coefficient with latitude.

3.1.2. Modelling tidal lagoons in TELEMAC

We represent each TRS in TELEMAC-2D using the T2D-TRS package[12] – a set of user-friendly subroutines designed for simulating the operation of TRSs (as described in [61], based on the work of [21]). T2D-TRS is based on the domain decomposition method, an approach consistent with other tidal range energy modelling studies (e.g. [62]) – the intricacies of this method are described in detail by Angeloudis et al. [63]. The TRS impoundment was implemented as a subdomain, culverts connect the impoundment subdomain to the ocean domain and transfer water between basins. Through modification of TELEMAC subroutines (`BUSE.f` – which was initially design to simulate culvert flow) and the development of a new subroutine (`T2D-TRS.f`), the activation of each culvert is controlled and the discharge is parameterised, in accordance with approximations of flow through turbines and sluice gates.

The typical method of turbine parameterisation uses a turbine specific Hill chart which relates power output P (W) and discharge Q ($m^3\ s^{-1}$) to the hydraulic head H (m; e.g. [64]). We implement a parameterisation which is based on a digitised Hill chart for the 9 m diameter Andritz Hydro double regulated bulb turbine (the most recent publicly available Hill chart; [65]). Using a linear-scaling method described in Eq. (1) (implemented in [66], developed by [65]), Q and P are scaled-down[13] to a diameter D = 7.2 m (to retain consistency with the optimised layout for the NWTL by [67]) — the scaled Hill chart is shown in Supplementary Fig. S2.

$$Q_{scaled} = Q_{base} \times \frac{{D_{scaled}}^2}{{D_{base}}^2} \tag{1}$$

Following the recommendation by Baker [68], sluice gates are parameterised by using the Orifice equation (Eq. (2)). Sluice gate discharge Q_{sl} is related to the discharge coefficient C_d (=1.0, consistent with the sensitivity study by [69]), sluice area A_s (=100 m^2) and varying head difference ΔH (m) between the surface elevation of the impoundment η_i and the ocean basin η_o.

$$Q_s = C_d A_s \sqrt{2g\Delta H} \tag{2}$$

The following constraints are applied to the layout of the TRS structures: (1) the embankment cannot be placed in water depths >30 m (embankment construction costs are prohibitive in deeper waters; [6]), and (2) turbines and sluice gates must be sited in water depths >10 m and >5 m, respectively.

The first tidal lagoon design (Table 1, S1) is based on the layout originally proposed by North Wales Tidal Energy [14], and later optimised by Xue [67], where A_s = 150 km^2 and the number of turbines N_t = 150. Subsequent scenarios implement smaller tidal lagoons with a layout based on S1 (shown in Fig. 4), A_s is reduced to $\approx \frac{5}{6}A_s$, $\frac{4}{6}A_s$, $\frac{3}{6}A_s$, $\frac{2}{6}A_s$ and $\frac{1}{6}A_s$. Because the rated theoretical power output varies linearly with the area of the impoundment ($P = A_s H^2$; [6]), the same scaling approach is applied to N_t. The number of sluice gates (N_s) has minimal influence on the power output [20], and meso-scale hydrodynamic impact of bi-directional tidal lagoons, hence we use N_s = 7 for all scenarios.

Each tidal lagoon operates in a two-way fixed-head mode (shown in Fig. 3 and further described by [64]), turbine operation was initiated when ΔH > 3.7 m, with operation ceasing when ΔH < 1.4 m (these are the optimal values for the NWTL (S1), found by [67]). To accurately mimic TRS operation, a non-linear ramp function is used to gradually open and close the sluice gates/turbines. The opening operation was given by a half-sinusoidal function: $f = sin(\pi \frac{t}{2T})$, $0 < t \leq T$, and the closing operation is given by a half cosine function: $f = cos(\pi \frac{t}{2T})$, $0 < t \leq T$ [70], where T = 0.5 is the time of opening and closing (in

[7] https://emodnet.ec.europa.eu/geoviewer/.
[8] https://lle.gov.wales/.
[9] https://www.imardis.org/.
[10] https://digimap.edina.ac.uk/.
[11] https://www.supercomputing.wales/.
[12] https://github.com/NHanousek/T2D-TRS.
[13] (P is scaled using the same method applied to Q.)

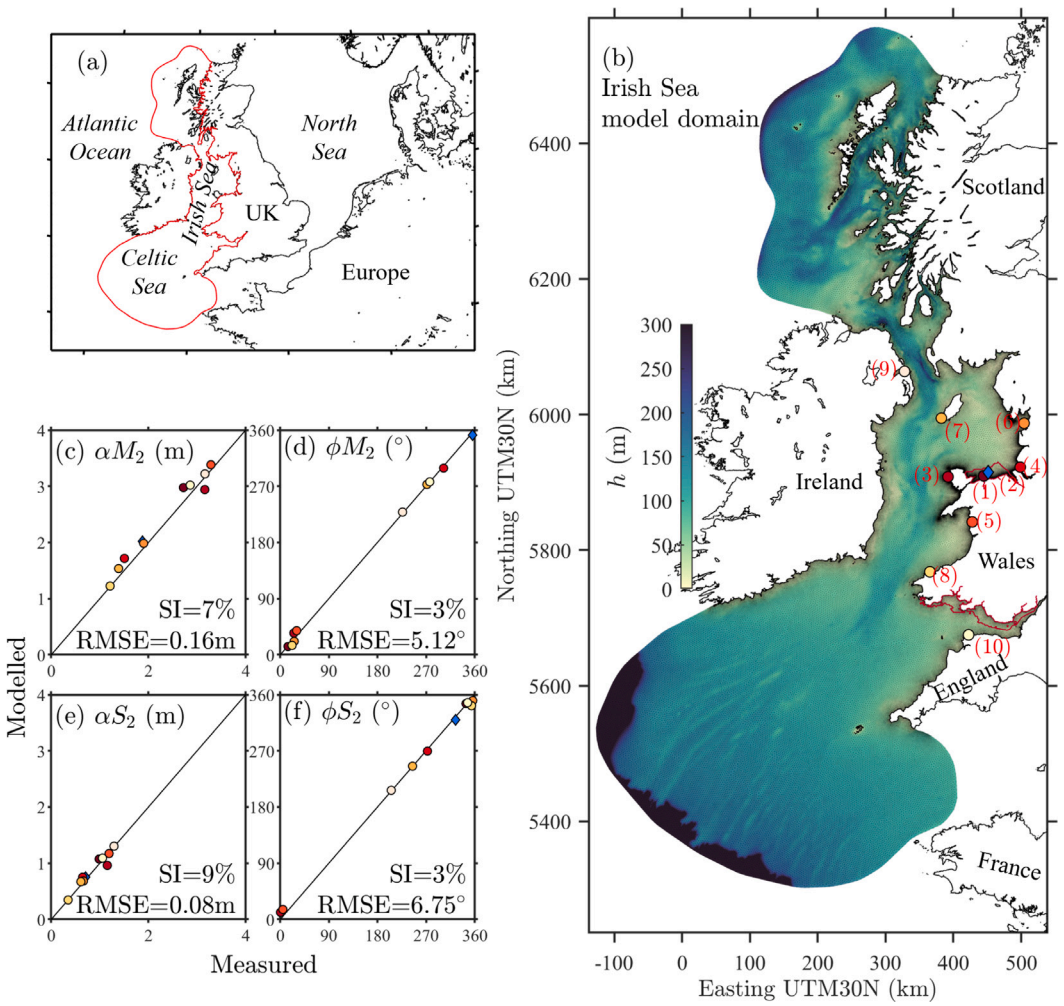

Fig. 2. (a) The red line outlines the model domain in the context of the North West European Shelf. (b) The baseline (no tidal lagoons) Irish Sea model domain showing the water depth h and mesh configuration. The circular markers in (b) show the location of the tidal gauges, the blue diamond marker shows the location of the ADCP deployment. In (b), the area contoured by the red line denotes the Welsh tidal range resource [60]. Scatter plots (c, d, e, f) show the correlation between observed and predicted tidal constituents at each validation site.

Table 1
TRS characteristics for each scenario. L_e is embankment length, V_i is impoundment volume, P_{max} is the installed capacity, $\overline{P}$ is the average power output for each tidal lagoon and $\overline{Q}$ is the mean turbine discharge (calculated over the 30-day simulation period). Consistent with findings from Cornett et al. [23], the relationship between A_s and $\overline{P}$ demonstrates a positive linear correlation. Due to the complex nature of coastal-seabed topography, V_i does not always exhibit a strong correlation with A_s.

Scenario	A_s (km^2)	L_e (km)	V_i (km^3)	N_t	N_S	P_{max} (MW)	$\overline{P}$ (MW)	$\overline{Q}$ m^3 s^{-1}
S0 (Baseline)	–	–		–	–	–	–	
S1	154.2	33.5	1.5	150	7	2,000	415	23,170
S2	124.9	30	1.1	125	7	1,690	355	19,360
S3	98.8	24.4	0.9	100	7	1,460	302	15,940
S4	75.1	22	0.6	75	7	1,030	221	11,910
S5	50.8	17	0.4	50	7	690	151	7,980
S6	25.3	11.6	0.2	25	7	340	77	3,870

hours).[14] The discharge and power output from the array of turbines in each tidal lagoon is presented in Supplementary Fig. S3.

[14] In reality the opening and closing time would be around 5–10 min, we use 30 min to ensure numerical stability and to eliminate water level oscillations.

3.2. Calibration and validation

A timeseries of water level measured at nine tidal gauge stations [28] and 48 ADCP deployment sites were used to calibrate and validate the simulated free surface elevation η and depth-averaged velocity components u, v (at each validation station, marked in Fig. 2b). Model calibration involved tuning the Manning's coefficient to minimise the difference between the measured and observed amplitude α and phase ϕ for the M_2 and S_2 harmonics. A Manning's value of 0.03 produced optimal $RMSE$ of 5.12° and 6.75° for $\overline{\phi_{M2}}$ and $\overline{\phi_{S2}}$ and 0.16 m and 0.08 m for $\overline{\alpha_{M2}}$ and $\overline{\alpha_{S2}}$ (complete calibration results are presented in Supplementary Table S1 and S2). Two error metrics, root-mean-squared error $RMSE$ (Eq. (3)) and scatter index SI (Eq. (4)), were used to quantify predictive performance:

$$\mathrm{RMSE} = \sqrt{\frac{1}{n}\sum_{i=1}^{n}(O_i - P_i)^2} \tag{3}$$

$$\mathrm{SI} = \frac{\mathrm{RMSE}}{\overline{O}} \times 100 \tag{4}$$

where O_i is the ith observation, P_i is the ith prediction, $\overline{O}$ is the mean of the observations, and $\overline{P}$ is the mean of the predictions.

Validation results for the M_2 and S_2 harmonics at each station are presented in Fig. 2c, d, e and f. The five principle constituents are validated at the ADCP deployment site, results are presented in Table 2.

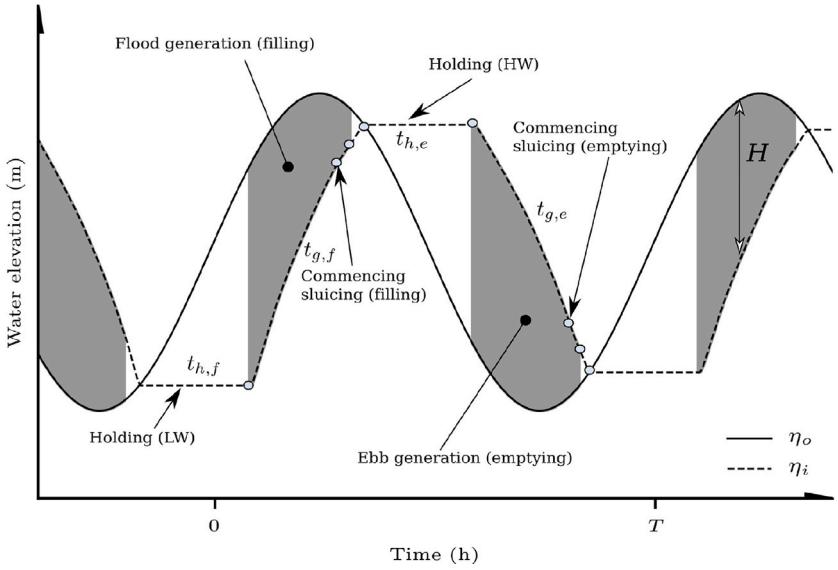

Fig. 3. The sequence of turbine and sluice gate operation for a two-way TRS, with a fixed head and excluding pumping. Key control variables are the flood holding $t_{h,f}$, ebb holding $t_{h,e}$, flood generation $t_{g,f}$ and ebb generation $t_{g,e}$ periods.
Source: From [71].

Table 2
Validation results for amplitude and phase of the five principle tidal constituents at the ADCP deployment site.

Amplitude α	M_2	S_2	O_1	K_1	N_2
Measured (m)	3.02	1.09	0.10	0.09	0.37
Modelled (m)	2.86	1.05	0.10	0.08	0.42
Difference (Δm)	−0.16	−0.04	0.00	−0.01	0.05
Difference (Δ%)	−5.34	−3.30	1.73	−6.71	12.55
Phase ϕ					
Measured (°)	277.07	347.14	251.80	258.52	324.78
Modelled (°)	276.83	346.87	248.39	264.30	319.08
Difference (Δ°)	−0.25	−0.27	−3.40	5.78	−5.69
Difference (Δ%)	−0.09	−0.08	−1.35	2.24	−1.75

Results are comparable with recent 2D hydrodynamic models for the region (e.g. Refs. [20,38,72]). Detailed station-specific validation results are given in the Supplementary Table S3.

3.3. Quantifying the impact of tidal lagoon impoundment size

Variations in the lagoon layout in each model scenario leads to differences in the model grid distribution between simulations. To ascertain the change Δ induced by a tidal lagoon, we linearly interpolate the model outputs: free surface elevation η, total water depth h ($h_{MSL} + \eta$, where h_{MSL} is the initial undisturbed water depth at MSL) and depth-averaged velocity components u, v onto regular 1 × 1 km grids at a 30 min time step (a suitable compromise which displays changes at the appropriate resolution, whilst representing the typical grid spacing). The data grid for the ambient (baseline) scenario (S0) is then subtracted from each of the other tidal lagoon scenarios (S1–S6). We compare the magnitude of impacts between scenarios at various locations, by extracting a timeseries at the desired location using a nearest-neighbour interpolation. To further analyse the model outputs, we calculate additional parameters:

1. *Harmonic constituents*: Harmonic analysis is used to deconstruct the timeseries of η at each node into the harmonic constituents using the T_TIDE package [73] with MATLAB R2023a.
2. *Bed shear stress*: We calculate bed shear stress τ_b (kg m^{-1}s^{-2}) using the Manning equation, implemented in BlueKenue [55]:

$$\frac{\tau_b}{\rho} = gn^2 \frac{|\mathbf{u}|\mathbf{u}}{D^{\frac{1}{3}}} \quad (5)$$

where ρ is seawater density (kg m^{-3}), $\mathbf{u}$ is depth-averaged velocity (= $\sqrt{u^2 + v^2}$, u and v are the horizontal velocity components; m s^{-1}), D is total water depth (m), n is Manning's coefficient (s m$^{-\frac{1}{3}}$) and g is acceleration due to gravity (=9.81 m s^{-2}).

4. Results and discussion

4.1. Impact on water levels

To better understand the impacts of tidal lagoon operation on tidal conditions, η can be deconstructed into the amplitude α and phase ϕ of the principle tidal constituents. Since M_2 is the dominant tidal constituent – it explains 58% of the observed tidal range, in the region of study – we present the predicted change $\Delta\alpha_{M2}$ and $\Delta\phi_{M2}$ for each tidal lagoon scenario in Figs. 5 and 6, respectively. In addition, we present amplitude and phase changes for S_2, N_2, O_1, K_1, M_4 and M_6 in the Supplementary Material.

Our simulations indicate that the general pattern of α_{M2} and ϕ_{M2} amplification/suppression remains largely the same for scenarios S1 to S6 (Figs. 5 and 6). A similar pattern is exhibited for the other semi-diurnal constituents (Supplementary Fig. S4, S5, S10 and S11). The largest tidal lagoon (S1) increases α_{M2} by 1 – 3 cm in the western Irish Sea, whilst reducing α_{M2} by 1 – 2 cm in the vicinity of the tidal lagoon (eastern Irish Sea), along the southeast coast of Ireland, in the Bristol Channel and in Cardigan Bay. All simulated changes are within the range of uncertainty for α_{M2} (Fig. 2). In the Bristol Channel, the $\Delta\alpha_{M2}$ caused by S2 is unexpectedly small (outlying the general trend; Fig. 5b), however it induces a large reduction in $\Delta\alpha_{M2}$ in the near-field (i.e. Solway Firth shown in Fig. 7).

The spatial distribution of our results ($\Delta\alpha_{M2}$) are consistent with those presented by Guo [62] when simulating the NWTL (similar in design to S1). Wolf et al. [74] and Yates et al. [75] also reported a similar pattern of $\Delta\alpha_{M2}$ when simulating numerous TRS in the Irish Sea (including barrages and lagoons). Results presented by Mackie

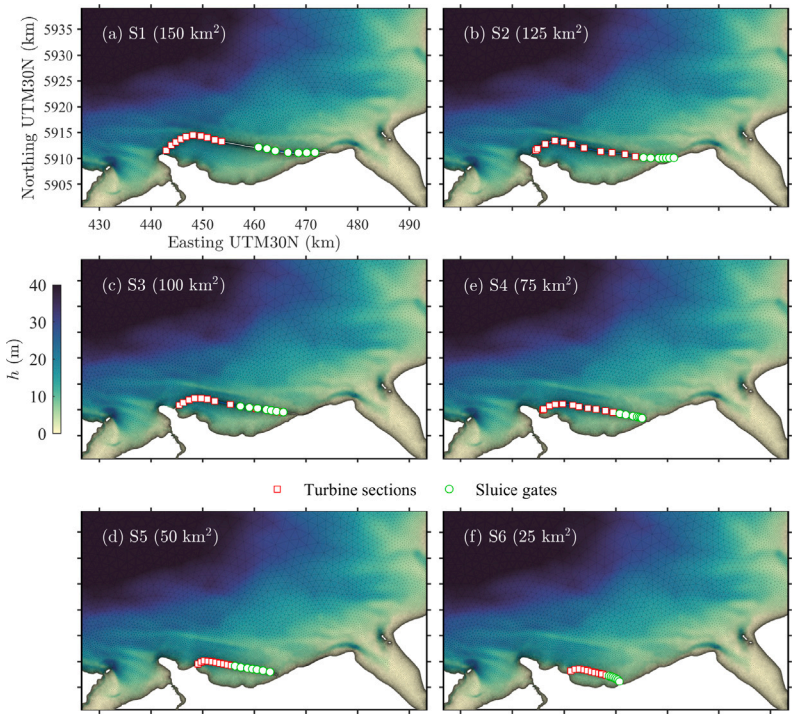

Fig. 4. Plots (a)–(f) show the layout of the embankment, turbines (red squares) and sluice gates (green circles) for each tidal lagoon scenario. The sensitivity of hydrodynamic impacts to the turbine and sluice gate layout was tested, the changes induced were of insignificant magnitude and constrained to the near-field. Water depth h is relative to MSL.

et al. [20] exhibit the closest agreement with our findings, when simulating the combined effects of four Irish Sea tidal lagoons, located at Conwy, Blackpool, Liverpool and Solway Firth (with a combined A_s = 160 km^2). However, direct comparisons with the literature are difficult due to discrepancies in (1) modelling approach (e.g. mesh resolution, open boundary location, friction parameterisations, and simulation time period), and (2) TRS configuration (e.g. location, layout, and operational scheme).

The eastern Irish Sea and Bristol Channel can be particularly sensitive to changes in tidal dynamics due to near resonance with the semi-diurnal constituents. A tidal lagoon on the North Wales coast reduces the width of the eastern Irish Sea which has a dampening effect on the incident tidal wave (for the semi-diurnal constituents); slowing the propagation speed and reducing the phase (as shown in Fig. 6). Since the eastern Irish Sea is approaching quarter wavelength resonance with the shelf (standing wave system; [76]), reducing the phase will move the system away from resonance (this phenomenon occurs for each of the semi-diurnal constituents, shown in Fig. 5 and Supplementary Fig. S4 and S5). For TRSs sited in more constrained water bodies, such as the Bristol Channel/Severn Estuary, this process will be more significant, causing larger perturbations to tidal dynamics (e.g. Refs. [11,21,77]). This relates to the concept of *blockage* which is described in detail by Mackie et al. [20].

To quantify the changes to the principle harmonic constituents, we compute the spatial average $\Delta\overline{\alpha}$ and absolute $\Delta\overline{|\alpha|}$ (Figs. 7 and 8, respectively) over three areas (defined in Fig. 5a). The amplitude of the semi-diurnal constituents (M_2, S_2 and N_2) is elevated in the far-field (defined as within a 200 km radius of the TRS), $\overline{\alpha_{M2S2N2}}$ increases from $0.1\% \leq \overline{\alpha_{M2S2N2}} \leq 0.3\%$ (S6) to $0.4\% \leq \overline{\alpha_{M2S2N2}} \leq 0.5\%$ (S1). In the near-field (within a 50 km radius), the percentage change in $\overline{\alpha_{M2S2N2}}$ values reduces from $-0.2\% \leq \overline{\alpha_{M2S2N2}} \leq -0.1\%$ (S6) to $-0.4\% \leq \overline{\alpha_{M2S2N2}} \leq -0.35\%$ (S1; Fig. 7b). In agreement with Cornett et al. [23], we find a strong linear correlation between far-field $\overline{\Delta\alpha_{M2S2}}$ and tidal lagoon characteristics (Table 3), and to a lesser extent in the near-field (S3 and S1 outlie this trend). S3 and S1 are the optimal scenarios to minimise near-field semi-diurnal constituent disturbances,

Table 3
Correlation coefficient R scores between the $\Delta\overline{|\alpha|}$ of principle harmonic constituents (and $\overline{|\eta_{max}|}$) and tidal lagoon characteristics: mean power output $\overline{P}$, mean turbine discharge $\overline{Q}$, impoundment surface area A_s and impoundment volume V_i (calculated over the 30-day simulation period at MSL).

	Far-field (200 km)				Near-field (50 km)			
	$\overline{P}$	$\overline{Q}$	A_s	V_i	$\overline{P}$	$\overline{Q}$	A_s	V_i
$\Delta\overline{\lvert\alpha_{M2}\rvert}$	0.97	0.97	0.98	**0.99**	0.70	**0.70**	0.70	0.67
$\Delta\overline{\lvert\alpha_{S2}\rvert}$	0.96	0.97	0.98	**0.98**	0.83	**0.90**	0.84	0.86
$\Delta\overline{\lvert\alpha_{N2}\rvert}$	0.89	0.90	0.89	**0.91**	0.85	0.86	0.86	0.84
$\Delta\overline{\lvert\alpha_{K1}\rvert}$	0.41	**0.41**	0.40	0.38	**0.49**	0.48	0.46	0.41
$\Delta\overline{\lvert\alpha_{O1}\rvert}$	**0.34**	0.33	0.31	0.29	**0.64**	0.63	0.61	0.57
$\Delta\overline{\lvert\eta_{max}\rvert}$	0.94	0.95	0.96	**0.97**	**0.95**	0.95	0.94	0.92

and thus $\Delta\eta_{max}$. Impoundment volume V_i has the strongest correlation with far-field $\Delta\overline{|\alpha_{M2S2N2}|}$ and $\Delta\overline{|\eta_{max}|}$ (Table 3). Near-field changes have a stronger correlation with $\overline{P}$ and $\overline{Q}$, perhaps owing to the locally constrained effects of turbine discharge.

In scenario S2, the tidal lagoon has the unique effect of minimising the disturbance to the amplitude of the diurnal constituents (K_1 and O_1), across all regions (Fig. 7, further supported by Fig. 8). The far-field reduction in the amplitude of diurnal constituents slightly diminishes the impact of the semi-diurnal amplitudes, having a reductive effect on η_{max}. Similar interactions are evident in the near-field, however the reduction is of a smaller magnitude, and the $\Delta\overline{|\alpha|}$ of semi-diurnal constituents reaches a maximum for all scenarios. For the diurnal constituents (O_1 and K_1), far-field $\Delta\overline{|\alpha|}$ is poorly correlated with the tidal lagoon characteristics presented in Table 3, however the correlation does slightly increase in the near-field.

The spatial pattern of $\Delta\eta_{max}$ is presented in Fig. 9. These changes are a product of the combined interaction of the modified harmonic constituents and, as the dominant constituent, $\Delta\alpha_{M2}$ strongly modulates $\Delta\eta_{max}$ (cf Fig. 5). However, in the Cardigan Bay region the $\Delta\eta_{max}$ is significantly less than $\Delta\alpha_{M2}$, because the $\Delta\alpha_{O1K1}$ (diurnal constituents) are suppressing $\Delta\eta_{max}$ (Supplementary Fig. S6 and S7).

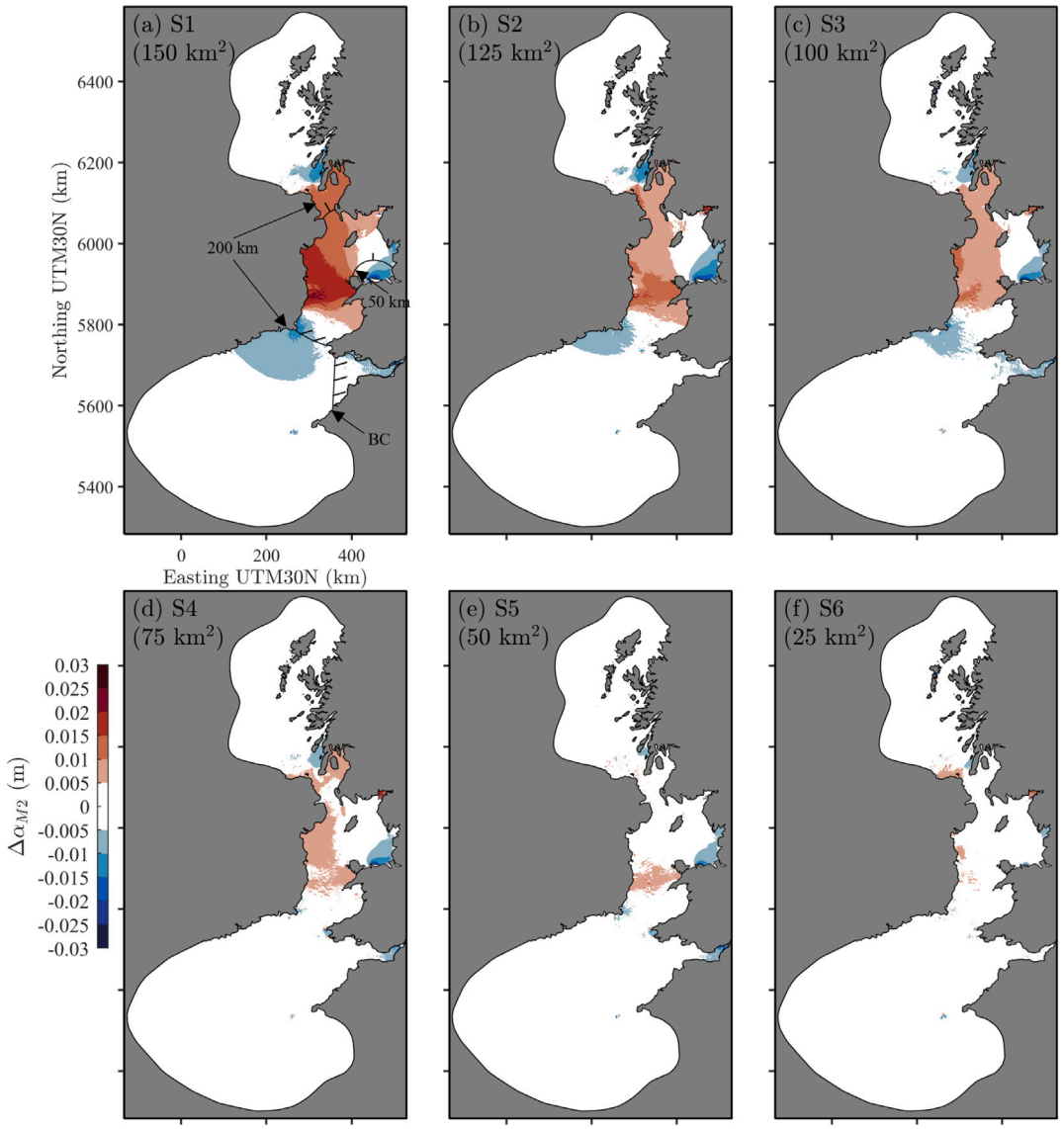

Fig. 5. The predicted change in the amplitude of the M_2 constituent $\Delta\alpha_{M2}$ (m), under each scenario (a) S1, (b) S2, (c) S3, (d) S4, (e) S5 and (f) S6. The results are interpolated to a 1 × 1 km grid for visualisation. In (a), the 50 km, 200 km and Bristol Channel (BC) regions are defined, these areas are referred to in Figs. 7 and 8.

Simulations by Guo [62] for the largest tidal lagoon (S1) somewhat agree with our results, although they only present near-field results, making a direct comparison difficult. Guo [62] also predicted a reduction in η_{max} between $5 < \eta_{max} < 10$ cm in Liverpool Bay, whereas our model predicts $2 < \eta_{max} < 3$ cm, therefore there is a considerable difference in the magnitude of the prediction. Furthermore, Guo [62] predicted a decrease in η_{max} across the Cardigan Bay region (between $5 < \eta_{max} < 10$ cm); such a decrease is not evident in our results and may be attributed to the different operational schemes used. Guo [62] operates the TRS using a flexible head setup, which ensures continuous operation throughout the neap tides, and therefore the TRS is operating for a larger proportion of the simulation period and potentially causing more extreme hydrodynamic impacts. Conversely, our fixed head setup results in a 'no generation' period at the peak of both neap tides (Supplementary Fig. S3).

The relationships quantified in Table 3 imply that reducing the far-field $\Delta\overline{|\eta_{max}|}$ (whilst maintaining $\overline{P}$) could be achieved by minimising V_i. Because $P \propto A_s H^2$ (where P is the instantaneous potential power; [78]). V_i can be reduced at no cost to electricity generation as long as it does not affect the tidal prism volume ($= H^* A_s$). Withholding a larger volume of water reduces the area into which the incoming tidal wave can propagate. An idealised impoundment maximises A_s, whilst ensuring the water depth across the majority of the impounded region does not drastically exceed practical limits.[15] The impoundment of these deeper regions does not benefit the TRS power output, and increases hydro-environmental impact (by occupying a larger volume of ocean), therefore they should be minimised. Our results indicate that reducing near-field changes (whilst maximising $\overline{P}$) presents a more significant challenge because $\Delta\overline{|\eta_{max}|}$ is strongly correlated with mean turbine discharge $\overline{Q}$ in this region, although some reduction in near-field change may occur through the minimisation of V_i. This relationship can be attributed to the locally-constrained nature of Q (which will increase water levels).

Table 4 presents $\Delta\eta_{max}$ at other suitable Irish Sea tidal lagoon sites (L1–L6), major docks (D1–D4) and communities vulnerable to coastal flooding (F1–F6), each of which are located in Fig. 9a. At Porthmadog, Solway Firth, Dublin, Belfast, and Dundalk, η_{max} is predicted to increase by >3 cm. These changes may seem insignificant, however,

[15] The depths required to site low-head hydro electric turbines and sluices gates, often cited as 10 m and 5 m, respectively.

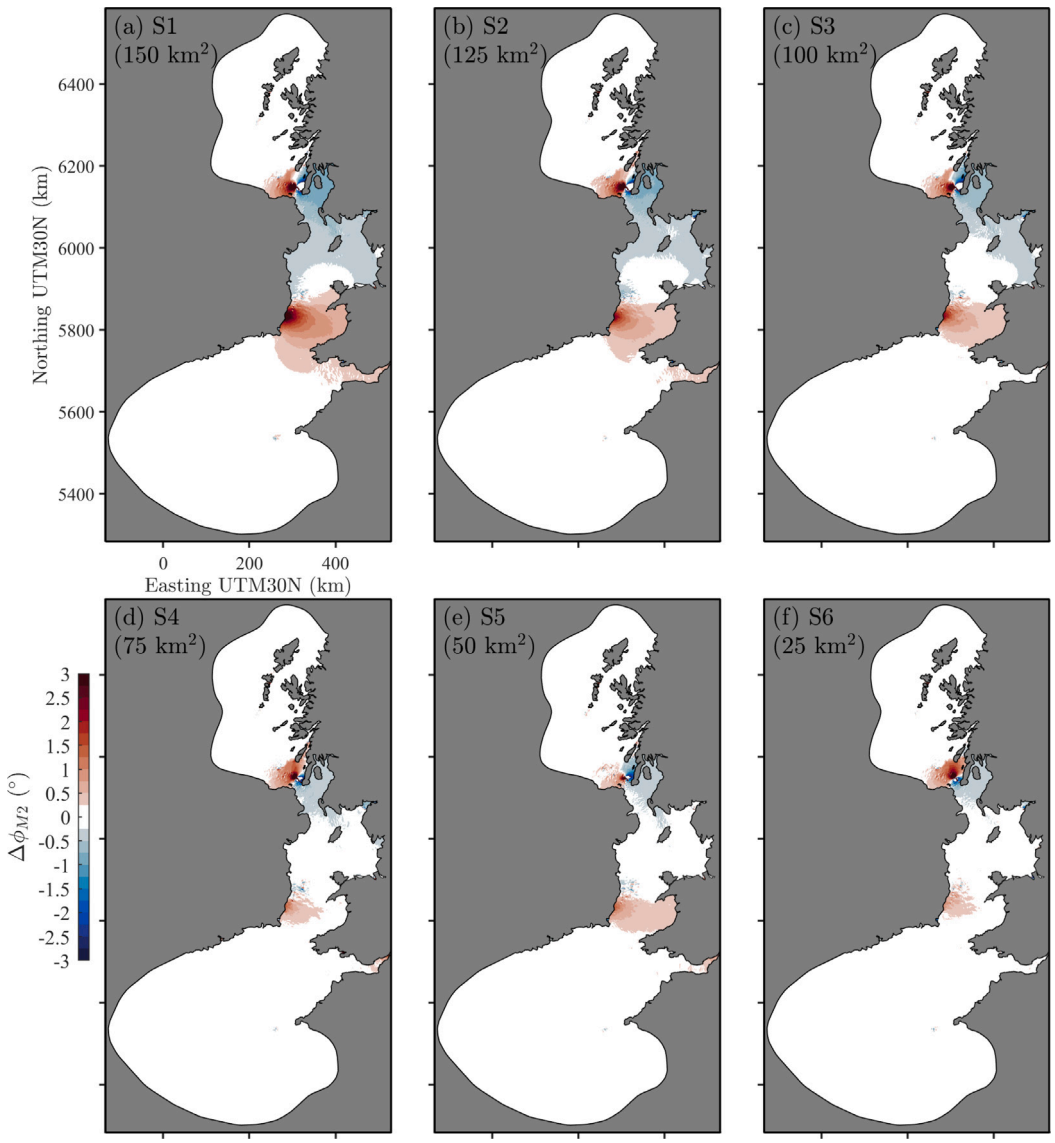

Fig. 6. The predicted change in the phase of the M_2 constituent $\Delta\phi_{M2}$ (°). Under each scenario (a) S1, (b) S2, (c) S3, (d) S4, (e) S5 and (f) S6, the results are interpolated to a 1 × 1 km grid for visualisation.

when coupled with: a surge component, extreme waves, and a rising MSL, small increases in tidal amplitude can exacerbate coastal flood risk through non-linear interactions [79]. This is especially relevant for locations where the relative change is larger (e.g. Dundalk and Belfast where $\Delta\eta_{max}$ = 2.03% and 1.02%, respectively; Table 4). The mean absolute change across all sites (Fig. 9, RMS) shows a positive correlation between hydrodynamic impact and tidal lagoon impounded size.

Under scenarios S1 and S2, the largest change in η_{max} is experienced at most sites (with the exception of Swansea and Watchey, in the Bristol Channel). Scenario S1 has the greatest impact on sites further afield (e.g. D2, D3 and L5), whereas S2 induces the greatest change at near-field sites (e.g. F1). In each scenario, the simulated $\Delta\eta_{max}$ does not exceed 4 cm (the maximum increase, relative to baseline conditions, was 2.03% at Dundalk). Interestingly, the largest change in the Bristol Channel (locations L4 and L6) are experienced under scenario S5. Our scenarios (S1–S6) reduce η_{max} at five potential tidal lagoon sites (L1, L2, L4, L5 and L6), decreasing the available tidal range resource. Since scenario S2 induces the strongest near-field changes, it will cause the largest reduction in the available tidal range resource at eastern Irish Sea tidal lagoon sites. Whereas at site L3 (Solway Firth), NWTL scenarios S1–S6 positively interact with η_{max} (this is supported by the pattern observed in Fig. 5).

4.2. Impact on tidal currents

In the far-field regions, each scenario has similar implications for $\Delta|U_{max}|$. Alternating patches of increased and reduced $\Delta|U_{max}|$ are present in the St Georges Channel, Bristol Channel, North Channel, and along the north of the Isle of Man. These regions could be associated with modifications to tidal phase and the slight shift in location of tidal currents. Near-field changes increase in magnitude with A_s (further evident in Fig. 11), whereas the nature of this relationship in the far-field is less clear. Cornett et al. [23] explored the link between hydro-environmental impact (namely, tidal range and current speed changes) and $\overline{P}$ for tidal lagoons in the Minas Basin, where simulated changes exhibited a strong linear correlation with the scale of development. These findings are mostly consistent with our results (in respect to water level changes, discussed in Section 4.1), however the results presented in Fig. 10 and Table 5 do not support this idea that changes in current speed exhibit a similar correlation. This could be attributed to the less constrained geometry, and lower tidal range, of the Irish Sea

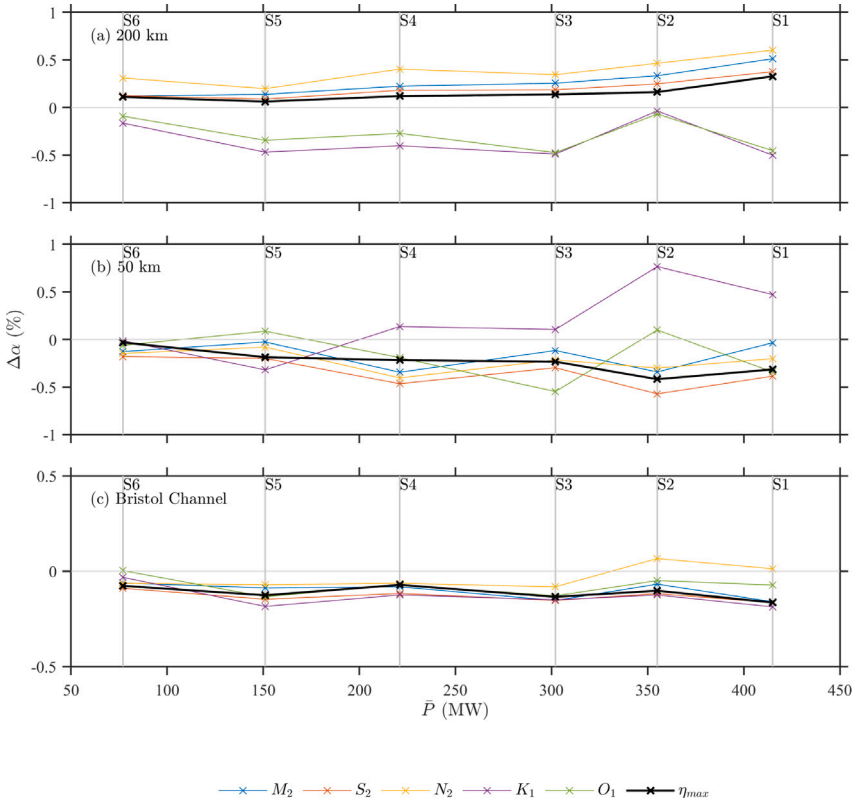

Fig. 7. The percentage change in amplitude $\Delta\overline{\alpha}$ of tidal constituents (and $\overline{\eta_{max}}$) averaged over various areas: (a) ≈200 km, and (b) ≈50 km in radius from each lagoon, and (c) the Bristol Channel (BC) region (shown in Fig. 5a). In each calculation, changes inside the lagoon impoundment are omitted. To reduce the effects of local extremes, which especially occur over inter-tidal regions, the 1 × 1 km grids were used for these calculations. Mean power output $\overline{P}$ is calculated over the 30-day simulation period.

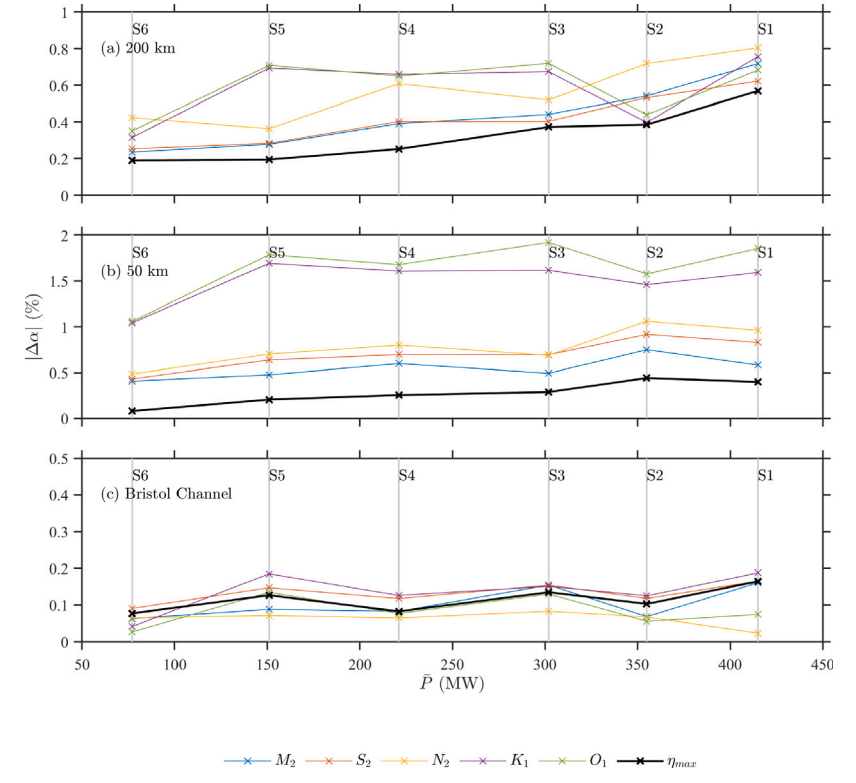

Fig. 8. Same as Fig. 7, but instead showing the absolute percentage change in amplitude $\Delta\overline{|\alpha|}$.

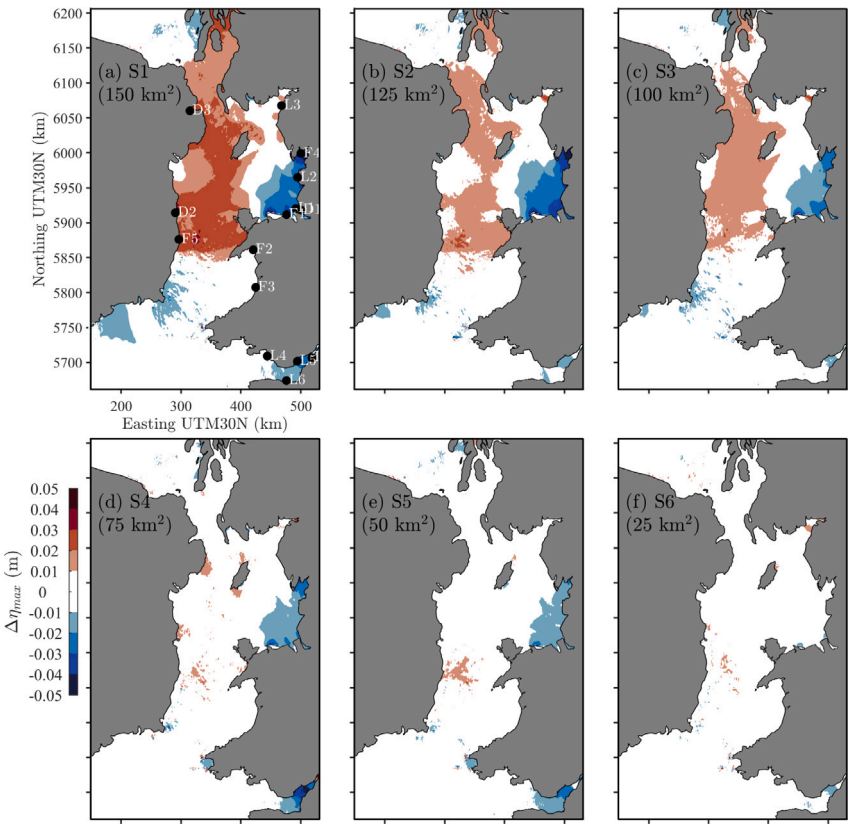

Fig. 9. Maximum changes in free surface elevation η_{max} (m) for each tidal lagoon scenario (a) S1, (b) S2, (c) S3, (d) S4, (e) S5 and (f) S6. In (a), the location of key sites (referred to in Table 4) are shown. Results are interpolated to a 1 × 1 km grid for visualisation.

Table 4
The change in maximum free surface elevation $\Delta\eta_{max}$ (m) simulated at various key locations in the Irish Sea (shown in Table 4a). The maximum values at each site are highlighted in bold. Percentage change Δ% (given in italics) is calculated relative to the baseline η_{max}.

		Proposed tidal lagoon sites						Major docks				Locations at risk of coastal flooding						
Site		Mersey	Blackpool	Solway	Swansea	Cardiff	Watchey	Liverpool	Dublin	Belfast	Bristol	Prestatyn	Porthmadog	Aberystwyth	Morcambe	Dundalk	Cork	
Site ID		L1	L2	L3	L4	L5	L6	D1	D2	D3	D4	F1	F2	F3	F4	F5	F6	
Lat (°)		53.43	53.83	54.75	51.53	51.47	51.47	53.41	53.34	54.65	51.51	53.35	52.9	52.41	54.14	53.00	51.76	
Lon (°)		−3.13	−3.08	−3.45	−3.81	−3.08	−3.34	−3.00	−6.15	−5.87	−2.73	−3.36	−4.18	−4.12	−3.00	−6.03	−8.25	
Scenario		Maximum free surface elevation η_{max}																RMS
S0	(m)	4.64	4.79	4.28	4.91	6.78	5.99	4.49	2.01	1.69	7.24	4.53	2.84	2.87	5.63	1.36	1.98	–
S1	Δ (m)	−0.02	−0.03	0	−0.01	**−0.02**	−0.02	−0.02	**0.01**	**0.02**	−0.01	−0.01	0	−0.01	−0.04	**0.03**	**−0.01**	0.016
S1	Δ (%)	*−0.39*	*−0.53*	*0.1*	*−0.16*	*−0.34*	*−0.26*	*−0.47*	*0.62*	*1.02*	*−0.14*	*−0.3*	*0.05*	*−0.19*	*−0.69*	*2.03*	*−0.44*	*0.483*
S2	Δ (m)	**−0.03**	**−0.03**	**0.01**	0	−0.01	−0.01	**−0.02**	0	0.01	0	**−0.03**	0	0	**−0.04**	0.01	−0.01	0.013
S2	Δ (%)	*−0.68*	*−0.63*	*0.15*	*−0.06*	*−0.21*	*−0.17*	*−0.52*	*0.1*	*0.76*	*−0.04*	*−0.56*	*0.16*	*−0.07*	*−0.73*	*0.86*	*−0.31*	*0.376*
S3	Δ (m)	−0.02	−0.02	0.01	0	−0.01	−0.01	−0.02	0.01	0.01	−0.01	−0.02	0	**−0.01**	−0.03	0.01	−0.01	0.0125
S3	Δ (%)	*−0.46*	*−0.4*	*0.15*	*−0.09*	*−0.15*	*−0.11*	*−0.34*	*0.38*	*0.58*	*−0.12*	*−0.33*	*−0.17*	*−0.31*	*−0.48*	*0.78*	*−0.32*	*0.323*
S4	Δ (m)	−0.01	−0.02	0.01	0	−0.03	−0.01	−0.01	0.01	0	**−0.02**	−0.02	**0.01**	0	−0.03	0	0	0.011
S4	Δ (%)	*−0.32*	*−0.36*	*0.14*	*−0.1*	*−0.48*	*−0.18*	*−0.24*	*0.25*	*−0.12*	*−0.33*	*−0.36*	*0.22*	*0*	*−0.51*	*0.19*	*0.22*	*0.251*
S5	Δ (m)	−0.02	−0.02	0	**−0.01**	−0.02	**−0.02**	−0.01	0	0	−0.01	−0.02	0	−0.01	−0.02	0.01	0	0.011
S5	Δ (%)	*−0.33*	*−0.32*	*0.03*	*−0.18*	*−0.33*	*−0.27*	*−0.23*	*0.13*	*0.19*	*−0.11*	*−0.43*	*−0.08*	*−0.2*	*−0.31*	*0.44*	*−0.18*	*0.235*
S6	Δ (m)	−0.01	−0.01	0.01	0	−0.01	−0.01	0	0.01	0	−0.01	−0.01	0	0	−0.01	0	0	0.006
S6	Δ (%)	*−0.21*	*−0.12*	*0.21*	*−0.09*	*−0.15*	*−0.15*	*−0.04*	*0.48*	*0.19*	*−0.07*	*−0.19*	*0.08*	*−0.11*	*−0.1*	*0.28*	*0.05*	*0.158*

(compared to the Minas Basin) which result in a lower blockage effect for Irish Sea tidal lagoons (cf Ref. [20]).

It is important to consider the impact of TRS on the resource availability of other sources of marine renewable energy. Tidal stream energy is rapidly developing and a number of sites are located in the Irish Sea [80], for example the recently announced 35 km^2 West Anglesey site is relatively close to the tidal lagoon site (shown in Fig. 1, TS1). Power generation is extremely sensitive to hydrodynamic conditions, thus seemingly trivial interactions could significantly reduce power output across an array of tidal stream turbines. For instance, a small change in current speed would have a significant impact, since $P \propto U^3$.

In Table 5, we examine the change in mean and maximum current speed ($|\overline{U}|$ and $|U_{max}|$, respectively) over three sites under scenarios S1-S6. The simulated $\Delta|\overline{U}|$ and $\Delta|U_{max}|$ are generally small (<1%) at the three sites, the largest $\Delta|U_{max}|$ is a decrease of 2 cm s^{-1} (0.311%) which occurs in S1. These results agree with those presented in Fig. 10, supporting the argument that the regions of significant current speed change are locally constrained. The results show a weak correlation between RMS Δ in $|\overline{U}|$ or $|U_{max}|$ and A_s. Analysis of the metrics presented in Table 5 suggests that the tidal lagoon design in S2 is the optimal scenario to minimise negative interference with the tidal stream resource (maximising $\overline{P}$, whilst minimising reduction in mean and maximum current speed over the three tidal stream sites considered).

4.2.1. Bed shear stress

Bed shear stress magnitude can be used as a proxy for seabed mobility, high bed shear stress occurs in shallow regions with high current speeds (Eq. (5)). In each tidal lagoon scenario (Fig. 11), $\Delta|\tau_{b\ max}|$ decreases at the western end of the structure, and this region extends further west (along the north coast of Anglesey) in the larger tidal lagoon scenarios. The structure impedes on the progression of the tidal wave around the Great Orme headland and into shallow coastal region

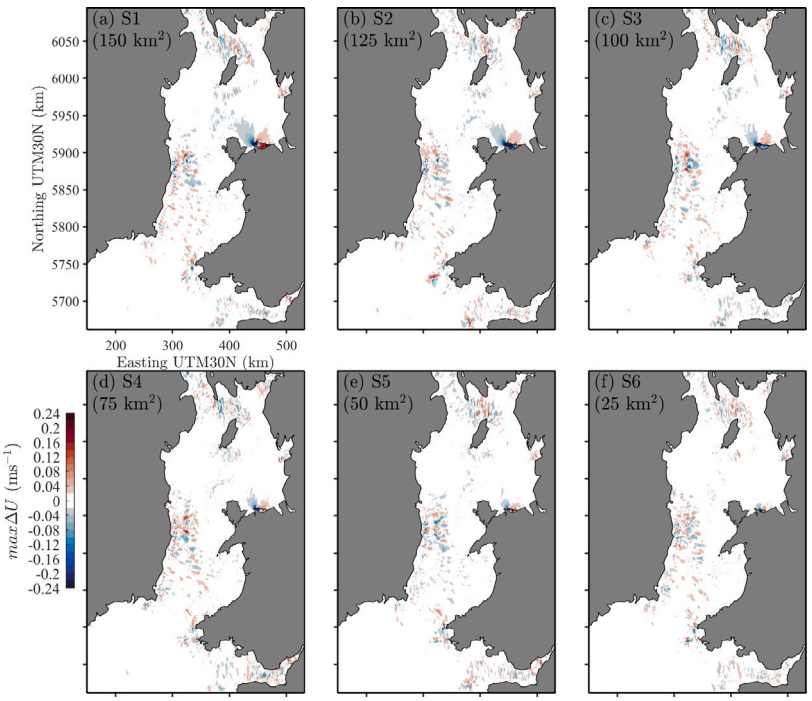

Fig. 10. The change in maximum current speed $\Delta|U_{max}|$ in each tidal lagoon scenario (a) S1, (b) S2, (c) S3, (d) S4, (e) S5 and (f) S6. Results are interpolated to a 1 × 1 km grid for visualisation.

Table 5
Change in magnitude of the mean and maximum tidal current speed ($\Delta|\overline{U}|$ and $\Delta|U_{max}|$, respectively) over the 30-day simulation period, changes are quantified at three tidal stream sites in the Irish Sea leased by the Crown Estate, the location of each site is shown in Fig. 1. The maximum values at each site is highlighted in bold. Percentage change (Δ%) is calculated relative to the baseline $|\overline{U}|$ and $|U_{max}|$, respectively.

		Tidal stream site							
	Site name	West Anglesey		Holyhead Deep		Bardsey Sound			
	Status	Consented		Consented		Pre-planning			
	Site ID	TS1		TS2		TS3			
	Lat (°)	53.30		53.31		52.77			
	Lon (°)	−4.73		−4.79		−4.78			
	Area (km)	35.04		9.17		3.34			
Scenario		$\overline{U}$	U_{max}	$\overline{U}$	U_{max}	$\overline{U}$	U_{max}	RMS $\overline{U}$	RMS U_{max}
S0	(m s^{-1})	1.23	2.54	0.99	2.15	1.34	2.64	–	–
S1	Δ (m s^{-1})	−0.00	0.00	0.00	−0.01	−0.01	−0.02	0.004	0.012
S1	Δ (%)	***−0.18***	*−0.09*	***−0.38***	***−0.64***	*−0.37*	***−0.78***	*0.311*	*0.503*
S2	Δ (m s^{-1})	0.00	0.00	0.00	−0.01	0.00	−0.01	0.002	0.006
S2	Δ (%)	*−0.13*	*−0.12*	*0.07*	*−0.39*	*−0.34*	*−0.26*	*0.178*	*0.255*
S3	Δ (m s^{-1})	0.00	0.00	0.00	−0.01	−0.01	−0.02	0.003	0.01
S3	Δ (%)	*0.01*	*0.10*	*−0.14*	*−0.38*	***−0.46***	*−0.73*	*0.203*	*0.404*
S4	Δ (m s^{-1})	0.00	0.01	0.00	0.00	−0.01	0.00	0.003	0.003
S4	Δ (%)	*0.07*	***0.29***	*0.23*	*0.10*	*−0.41*	*0.07*	*0.234*	*0.152*
S5	Δ (m s^{-1})	0.00	0.01	0.00	0.00	0.00	−0.01	0.002	0.004
S5	Δ (%)	*0.04*	*0.21*	*0.10*	*−0.02*	*−0.30*	*−0.26*	*0.145*	*0.163*
S6	Δ (m s^{-1})	0.00	0.01	0.00	0.00	0.00	−0.01	0.002	0.004
S6	Δ (%)	*−0.01*	*0.10*	*0.12*	*−0.16*	*0.16*	*0.44*	*0.095*	*0.234*

of Llandudno Bay and Rhos Bay, reducing tidal current speeds and therefore bed shear stress. Our simulations suggest that the sandbanks in Conwy Bay will experience reduced $|\tau_{b\ max}|$. These impacts scale closely with A_s, for example in S6 the region where $\Delta|\tau_{b\ max}| > 0.02$ does not extend west beyond the Great Orme (Fig. 11b). A similar, albeit smaller, region of reduced bed shear stress appears at the eastern end of the structure and in the Mersey estuary.

In agreement with previous TRS simulations (e.g. Refs. [20,62]), the seabed in the vicinity of the turbines experiences a dramatic increase in $|\tau_{b\ max}|$. Due to the offshore location of the embankment, in scenarios S1–S5 the turbine exit jets flow over Constable Bank (an important offshore sandbank from an ecological and coastal defence perspective), this is likely to result in localised scour over the bank and extensive morphological change. Guo [62] used a conventional quadratic stress law to calculate τ_b in the near-field region of the NWTL. Regions of high τ_b local to the turbines are consistent with Ref. [62], and the region of reduced $|\tau_{b\ max}|$ at the western end of the structure is supported by Mackie et al. [20] (from simulations of the Conwy lagoon, where A_s = 50 km^2).

4.3. Limitations

The TELEMAC-2D model used here is a two-dimensional (depth-averaged) model, forced only by tides. The model does not consider

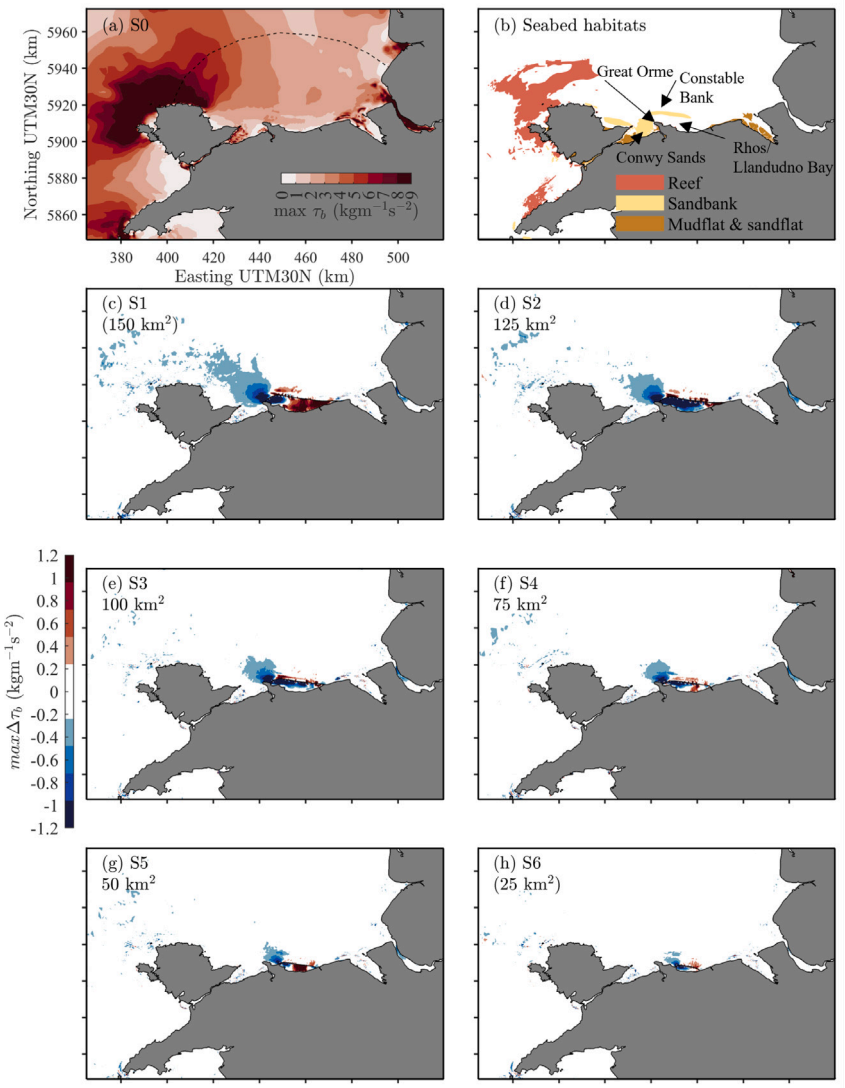

Fig. 11. The change in magnitude of maximum bed shear stress $\Delta|\tau_{b\ max}|$ for each tidal lagoon scenario (c) S1, (d) S2, (e) S3, (f) S4, (g), S5 and (h) S6. (a) Shows the bed shear stress in the baseline scenario (the dashed lined denotes the region within a 50 km radius of each tidal lagoon, referred to in Fig. 7). (b) Shows key benthic habitats located within Welsh waters (delineated by Natural Resources Wales; [60]), these features are sensitive to $\Delta|\tau_{b\ max}|$. Key locations are labelled in (b). Results are interpolated to a 250 × 250 m grid for visualisation.

baroclinic flows, wind/wave induced currents, freshwater inflows and atmospheric pressure. Based on previous research (e.g. [81]), we suspect that the interaction between a TRS and these physical mechanisms (i.e waves) would have insignificant effect on large scale hydrodynamics, therefore we choose to focus solely on depth-averaged tidal dynamics. Due to the computational demands and complexity of the 3D modelling technique, it is only necessary for studies which focus on the near-field impacts of TRSs [82] – to the authors' knowledge, previous shelf-scale simulations of TRSs have exclusively used 2D models. Current understanding of the 3D flow pattern caused by the turbine exit jets, suggests that it is only significant within 20D of the turbines (in our case, this is a distance of 144 m; [83]). Because our study focuses on impacts well in excess of this distance, we believe that neglecting these 3D flows will have a negligible impact on our overall findings.

Seabed roughness, which is the combined effect of seabed substrate roughness and bedform morphology, influences flow strength, turbulent mixing, bed shear stress and sediment transport. In our model, seabed roughness is parameterised using a spatially constant Manning's coefficient, whereas in reality the bed roughness varies in space and time. Future research may involve coupling this model with a morphodynamic/sediment transport module which includes a seabed sediment distribution (based on observations) and a parameterisation of spatio-temporal bedform roughness (as described in [84]).

In this study, each TRS use a fixed head setup, the number of turbines were scaled linearly with impoundment area and the number of sluice gates remained constant. When designing future TRSs, developers would maximise electricity output through use of 0D models to optimise the number and position of turbines and sluice gates. In addition, the TRS would use a flexible operational head, which has been shown to increases power output by up to 10% [85,86]. Introducing a flexible head operational mode in these simulations may increase the time-averaged impact of each lagoon, since it would remove the period of 'no generation' during neap tides (Supplementary Fig. S3). Optimising these aspects of the TRS was not within the scope of this study since it would introduce additional complexity, making it harder to isolate the individual effects of tidal lagoon size.

Pappas et al. [87] recently showed the importance of selecting a representative simulation period when conducting resource, and environmental impact, assessments for proposed TRS. In our study, we were constrained to within the measurement period of the ADCP deployment. Future studies could use only tidal gauges for validation and implement the method described by Pappas et al. [87], selecting

a tidal month which is representative of the long-term average tidal conditions.

5. Conclusions

In this study, we investigate the impact of a tidal lagoon impoundment area on tidal amplitudes and currents. We describe complex and distinct responses in the amplitude of the principle tidal constituents to the operation of tidal lagoons. A fully validated shelf-scale hydrodynamic model (tidal elevations and currents), based on the TELEMAC modelling system, is developed. The T2D-TRS package is implemented to simulate six hypothetical tidal lagoon scenarios. Located on the North Wales coast, each tidal lagoon has an impoundment area ranging from 25–150 km^2. From the discussion and analysis of our results, the following conclusions are drawn:

- The amplitude of semi-diurnal constituents M_2, S_2 and N_2 are reduced in the near-field (within a 50 km radius of the lagoon) and increased in the far-field (within a 200 km radius of the lagoon).
- In the most extreme scenario (a 150 km^2 lagoon impoundment area) maximum water levels are increased by 2–3 cm in the western Irish Sea, and reduced by 2–4 cm in the eastern Irish Sea, having implications for coastal flood risk, intertidal area extent and the potential tidal range energy resource at other sites.
- Modifications to the amplitudes of the diurnal-constituents O_1 and K_1 are around twice as large in the near-field, these changes weakly correlate with tidal lagoon characteristics, and have only a minor influence on water levels.
- Tidal lagoon impoundment volume exhibits the strongest correlation ($R = 0.97$) with the net far-field change in water levels, whereas the mean turbine discharge shows the strongest correlation ($R = 0.95$) in the near-field.
- Maximum depth-averaged tidal current speeds (and bed shear stresses) will reduce to the northwest of the structure (by ≈ 6 cm s^{-1}), whilst current speeds in the vicinity of the turbines will increase, which will likely modify key benthic habitats. Only trivial changes in the local tidal stream resource are noted.

Due to the enormous civil engineering challenge and substantial capital cost associated with developing a TRS, the use, and further development, of numerical models offers an excellent opportunity to predict hydro-environmental impacts prior to financial commitment. There is significant potential to optimise many aspects of TRSs, thus we identify the following directions for future research: (1) An application of the methodology used in this study (i.e. varying the TRS impoundment area) at tidal range energy sites located in enclosed basins (e.g. Bristol Channel; where changes to tidal dynamics will be more severe). (2) An investigation the impact of minimising impoundment volume, whilst keeping impoundment area constant (through site selection and embankment placement), we suspect that this may reduce hydro-environmental impacts (at no cost to power generation). (3) A study into the evolution of a TRS's interaction with a rising sea level, because TRSs are expected to operate for over a century, it is important that this is assessed.

CRediT authorship contribution statement

Edward Roome: Writing – review & editing, Writing – original draft, Visualization, Methodology, Investigation, Formal analysis, Data curation. **Peter Robins:** Writing – review & editing, Supervision, Conceptualization. **Reza Ahmadian:** Writing – review & editing. **Martin Austin:** Writing – review & editing, Supervision. **Nicolas Hanousek:** Writing – review & editing, Software. **Bin Guo:** Writing – review & editing, Software. **Simon Neill:** Writing – review & editing.

Declaration of competing interest

The authors declare that they have no known competing financial interests or personal relationships that could have appeared to influence the work reported in this paper.

Acknowledgements

We thank Preston Spicer (Pacific Northwest National Laboratory) and two anonymous reviewers who provided constructive comments on an earlier version of the manuscript. We appreciate the facilities provided by the Supercomputing Wales project, which is part-funded by the European Regional Development Fund (ERDF) via Welsh Government. We acknowledge the support from Alan G. Davies (Bangor University) for his initial conceptualisation of the project and insights into modelling the North Wales region. We are also thankful for the bathymetric data from the EMODnet bathymetry portal – https://emodnet.ec.europa.eu/geoviewer/. We acknowledge the support of NERC (National Environment Research Council), United Kingdom grant reference NE/V009109/1.

Appendix A. Supplementary data

Supplementary material related to this article can be found online at https://doi.org/10.1016/j.renene.2024.121601.

Data availability

The raw data presented in the figures will be made available on request.

References

[1] R. Newell, D. Raimi, G. Aldana, Global energy outlook 2019 : The next generation of energy, Resour. Future 1 (2019) 8–19.
[2] V. Ramanathan, Y. Feng, On avoiding dangerous anthropogenic interference with the climate system: Formidable challenges ahead, Proc. Natl. Acad. Sci. 105 (38) (2008) 14245–14250.
[3] S.E. Shmelev, J.C. Van Den Bergh, Optimal diversity of renewable energy alternatives under multiple criteria: An application to the UK, Renew. Sustain. Energy Rev. 60 (2016) 679–691.
[4] A.G. Borthwick, Marine renewable energy seascape, Engineering 2 (1) (2016) 69–78.
[5] V.M. Barclay, S.P. Neill, A. Angeloudis, Tidal range resource of the Patagonian Shelf, Renew. Energy 209 (2023) 85–96.
[6] S.P. Neill, A. Angeloudis, P.E. Robins, I. Walkington, S.L. Ward, I. Masters, M.J. Lewis, M. Piano, A. Avdis, M.D. Piggott, et al., Tidal range energy resource and optimization–past perspectives and future challenges, Renew. Energy 127 (2018) 763–778.
[7] S.P. Neill, The future of ocean renewable energy, in: Living with Climate Change, Elsevier, 2024, pp. 449–464.
[8] A. Etemadi, Y. Emami, O. AsefAfshar, A. Emdadi, Electricity generation by the tidal barrages, Energy Procedia 12 (2011) 928–935.
[9] S. Waters, G. Aggidis, Tidal range technologies and state of the art in review, Renew. Sustain. Energy Rev. 59 (2016) 514–529.
[10] S. Waters, G. Aggidis, A world first: Swansea Bay Tidal lagoon in review, Renew. Sustain. Energy Rev. 56 (2016) 916–921.
[11] J. Xia, R.A. Falconer, B. Lin, Impact of different operating modes for a Severn Barrage on the tidal power and flood inundation in the Severn Estuary, UK, Appl. Energy 87 (7) (2010) 2374–2391.
[12] W. Langston, P. Jonas, G. Millward, The Severn Estuary and Bristol Channel: A 25 year critical review, Mar. Pollut. Bull. 61 (1–3) (2010) 1–4.
[13] U.G. United Kingdom Government, Renewable sources of energy, chapter 6: Digest of united kingdom energy statistics (dukes), 2023, URL https://www.gov.uk/government/statistics/renewable-sources-of-energy-chapter-6-digest-of-united-kingdom-energy-statistics-dukes. (Accessed 19 February 2024).
[14] N.W.T.E. NWTE, North Wales presents a world-class site for a tidal lagoon, 2013, URL https://www.northwalestidalenergy.com/about. (Accessed 18 January 2024).
[15] C. Hendry, The role of tidal lagoons final report, 2016 (2017).

[16] New Civil Engineer, Innovation competition launched to solve tidal lagoon challenges, 2023, URL https://www.newcivilengineer.com/latest/innovation-competition-launched-to-solve-tidal-lagoon-challenges-30-06-2023/. (Accessed 12 June 2024).

[17] R. Burrows, I. Walkington, N. Yates, T. Hedges, J. Wolf, J. Holt, The tidal range energy potential of the West Coast of the United Kingdom, Appl. Ocean Res. 31 (4) (2009) 229–238.

[18] J.P. Frau, Tidal energy: promising projects: La rance, a successful industrial-scale experiment, IEEE Trans. Energy Convers. 8 (3) (1993) 552–558.

[19] C.V. Vouriot, A. Angeloudis, S.C. Kramer, M.D. Piggott, Fate of large-scale vortices in idealized tidal lagoons, Environ. Fluid Mech. 19 (2019) 329–348.

[20] L. Mackie, S.C. Kramer, M.D. Piggott, A. Angeloudis, Assessing impacts of tidal power lagoons of a consistent design, Ocean Eng. 240 (2021) 109879.

[21] B. Guo, R. Ahmadian, R.A. Falconer, Refined hydro-environmental modelling for tidal energy generation: West Somerset Lagoon case study, Renew. Energy 179 (2021) 2104–2123.

[22] K. Elliott, H.C. Smith, F. Moore, A.H. van der Weijde, I. Lazakis, Environmental interactions of tidal lagoons: A comparison of industry perspectives, Renew. Energy 119 (2018) 309–319.

[23] A. Cornett, J. Cousineau, I. Nistor, Assessment of hydrodynamic impacts from tidal power lagoons in the Bay of Fundy, Int. J. Mar. Energy 1 (2013) 33–54.

[24] J. Xue, R. Ahmadian, O. Jones, R.A. Falconer, Design of tidal range energy generation schemes using a Genetic Algorithm model, Appl. Energy 286 (2021) 116506.

[25] T. Zhang, N. Hanousek, M. Qadrdan, R. Ahmadian, A day-ahead scheduling model of power systems incorporating multiple tidal range power stations, IEEE Trans. Sustain. Energy 14 (2) (2022) 826–836.

[26] C. Leech, An Experimental Study of the Hydrodynamic Impact of Turbine Layout and Design Considerations in Tidal Range Schemes (Ph.D. thesis), Cardiff University, 2022.

[27] J.S. Pethick, R.K. Morris, D.H. Evans, Nature conservation implications of a Severn tidal barrage–a preliminary assessment of geomorphological change, J. Nat. Conserv. 17 (4) (2009) 183–198.

[28] C. BODC, UK tide gauge network data, 2017, URL https://www.bodc.ac.uk/.

[29] C. Lyddon, A. Plater, J. Brown, T. Prime, J. Wolf, The Impact of Tidal Lagoons on Future Flood Risk on the North Wirral and Conwy Coastline, UK, Tech. Rep., National Oceanography Centre, 2015.

[30] A.G. Davies, P. Robins, M. Austin, G. Walker-Springett, Exploring regional coastal sediment pathways using a coupled tide-wave-sediment dynamics model, Cont. Shelf Res. 253 (2023) 104903.

[31] D. Bowers, S. Gaffney, M. White, P. Bowyer, Turbidity in the southern Irish Sea, Cont. Shelf Res. 22 (15) (2002) 2115–2126.

[32] D. Bowers, S. Boudjelas, G. Harker, The distribution of fine suspended sediments in the surface waters of the Irish Sea and its relation to tidal stirring, Int. J. Remote Sens. 19 (14) (1998) 2789–2805.

[33] T. Dabrowski, M. Hartnett, Modelling travel and residence times in the eastern Irish Sea, Mar. Pollut. Bull. 57 (1–5) (2008) 41–46.

[34] J.A. Polton, M.R. Palmer, M.J. Howarth, Physical and dynamical oceanography of Liverpool Bay, Ocean Dyn. 61 (2011) 1421–1439.

[35] M.R. Palmer, J.A. Polton, A strain-induced freshwater pump in the Liverpool bay ROFI, Ocean Dyn. 61 (2011) 1905–1915.

[36] I. Robinson, The tidal dynamics of the Irish and Celtic Seas, Geophys. J. Int. 56 (1) (1979) 159–197.

[37] M. Howarth, Hydrography of the Irish Sea, Citeseer, 2005.

[38] J. Horrillo-Caraballo, Y. Yin, I. Fairley, H. Karunarathna, I. Masters, D. Reeve, A comprehensive study of the tides around the Welsh coastal waters, Estuarine, Coast. Shelf Sci. 254 (2021) 107326.

[39] J. Tinker, J.A. Polton, P.E. Robins, M.J. Lewis, C.K. O'Neill, The influence of tides on the North West European shelf winter residual circulation, Front. Mar. Sci. 9 (2022) 847138.

[40] J.M. Brown, D.L. Norman, L.O. Amoudry, A.J. Souza, Impact of operational model nesting approaches and inherent errors for coastal simulations, Ocean Model. 107 (2016) 48–63.

[41] S.P. Neill, Wave resource characterization and co-location with offshore wind in the Irish Sea, Renew. Energy 222 (2024) 119902.

[42] N. Kenyon, B. Cooper, Sand Banks, Sand Transport and Offshore Wind Farms, Kenyon MarineGeo, 2005.

[43] P. Amjadian, S.P. Neill, V. Martí Barclay, Characterizing seabed sediments at contrasting offshore renewable energy sites, Front. Mar. Sci. 10 (2023) 1156486.

[44] S.L. Ward, S.P. Neill, K.J. Van Landeghem, J.D. Scourse, Classifying seabed sediment type using simulated tidal-induced bed shear stress, Mar. Geol. 367 (2015) 94–104.

[45] C.A. Unsworth, M.J. Austin, K.J. Van Landeghem, A.J. Couldrey, R.J. Whitehouse, B. Lincoln, S. Doole, P. Worrall, Field measurements of cable self-burial in a sandy marine environment, Coast. Eng. 184 (2023) 104309.

[46] V. Masson-Delmotte, P. Zhai, A. Pirani, S.L. Connors, C. Péan, S. Berger, N. Caud, Y. Chen, L. Goldfarb, M. Gomis, et al., Climate change 2021: The physical science basis, Contribution of working group I to the sixth assessment report of the intergovernmental panel on climate change, 2 (2021).

[47] J.O. Pope, K. Brown, F. Fung, H.M. Hanlon, R. Neal, E.J. Palin, A. Reid, Investigation of future climate change over the British Isles using weather patterns, Clim. Dyn. 58 (9–10) (2022) 2405–2419.

[48] C. Lyddon, N. Chien, G. Vasilopoulos, M. Ridgill, S. Moradian, A. Olbert, T. Coulthard, A. Barkwith, P. Robins, Thresholds for estuarine compound flooding using a combined hydrodynamic–statistical modelling approach, Nat. Hazards Earth Syst. Sci. 24 (3) (2024) 973–997.

[49] S.P. Neill, J.D. Scourse, The formation of headland/island sandbanks, Cont. Shelf Res. 29 (18) (2009) 2167–2177.

[50] J.-M. Hervouet, Hydrodynamics of Free Surface Flows: Modelling with the Finite Element Method, John Wiley & Sons, 2007.

[51] B. Carroll, M. Li, S. Pan, J. Wolf, R. Burrows, Morphodynamic impacts of a tidal barrage in the Mersey Estuary, in: Coastal Engineering 2008, Vol. 5, World Scientific, 2009, pp. 2743–2755.

[52] B. Guo, R. Ahmadian, P. Evans, R.A. Falconer, Studying the wake of an island in a macro-tidal estuary, Water 12 (5) (2020) 1225.

[53] W.A. Breugem, Wetting and drying improvements in TELEMAC (part 1), in: XXVIIIth TELEMAC User Conference, 2022, p. 35.

[54] P. Mewis, A quasi bubble-function approach for shallow water waves, Adv. Hydro-Sci. Eng. 1 (1993) 768–774.

[55] CHC, Canadian Hydraulics Centre, Blue Kenue–reference manual, 2010, URL https://nrc.canada.ca/en/research-development/products-services/software-applications/blue-kenuetm-software-tool-hydraulic-modellers.

[56] G.D. Egbert, S.Y. Erofeeva, Efficient inverse modeling of barotropic ocean tides, J. Atmos. Ocean. Technol. 19 (2) (2002) 183–204.

[57] Q. Ma, T.A. Adcock, Modification of tidal resonance in the Severn Estuary by a barrage and lagoon, J. Ocean Eng. Mar. Energy 6 (2020) 171–181.

[58] J. Zhou, S. Pan, R.A. Falconer, Effects of open boundary location on the far-field hydrodynamics of a Severn Barrage, Ocean Model. 73 (2014) 19–29.

[59] P. Hadziabdic, L. Rickards, Review of the Irish Sea (Area 6) Oceanography, British Oceanographic Data Centre, 1999, pp. 1–135.

[60] DataMap Wales, DataMap Wales, 2022, URL https://datamap.gov.wales. (Accessed 16 January 2024).

[61] N. Hanousek, Numerical Modelling of Tidal Energy Devices and Structures As Part of Net Zero (Ph.D. thesis), Cardiff University, 2023.

[62] B. Guo, Hydro-Environmental Modelling and Interaction of Tidal Lagoons Around the UK Coast (Ph.D. thesis), Cardiff University, 2022.

[63] A. Angeloudis, R.A. Falconer, S. Bray, R. Ahmadian, Representation and operation of tidal energy impoundments in a coastal hydrodynamic model, Renew. Energy 99 (2016) 1103–1115.

[64] A. Angeloudis, R.A. Falconer, Sensitivity of tidal lagoon and barrage hydrodynamic impacts and energy outputs to operational characteristics, Renew. Energy 114 (2017) 337–351.

[65] G. Aggidis, O. Feather, Tidal range turbines and generation on the Solway Firth, Renew. Energy 43 (2012) 9–17.

[66] N. Hanousek, R. Ahmadian, E. Lesurf, Providing distributed electrical generation through retrofitting disused docks as tidal range energy schemes, Renew. Energy 217 (2023) 119149.

[67] J. Xue, Optimisation of Tidal Range Schemes (Ph.D. thesis), Cardiff University, 2021.

[68] C. Baker, Tidal power, Energy Policy 19 (8) (1991) 792–797.

[69] S. Bray, R. Ahmadian, R.A. Falconer, Impact of representation of hydraulic structures in modelling a Severn Barrage, Comput. Geosci. 89 (2016) 96–106.

[70] J. Zhou, S. Pan, R.A. Falconer, Optimization modelling of the impacts of a Severn Barrage for a two-way generation scheme using a Continental Shelf model, Renew. Energy 72 (2014) 415–427.

[71] A.L. Baker, R.M. Craighead, E.J. Jarvis, H.C. Stenton, A. Angeloudis, L. Mackie, A. Avdis, M.D. Piggott, J. Hill, Modelling the impact of tidal range energy on species communities, Ocean Coast. Manag. 193 (2020) 105221.

[72] P.E. Robins, S.P. Neill, M.J. Lewis, S.L. Ward, Characterising the spatial and temporal variability of the tidal-stream energy resource over the northwest european shelf seas, Appl. Energy 147 (2015) 510–522.

[73] R. Pawlowicz, B. Beardsley, S. Lentz, Classical tidal harmonic analysis including error estimates in MATLAB using T_TIDE, Comput. Geosci. 28 (8) (2002) 929–937.

[74] J. Wolf, I. Walkington, J. Holt, R. Burrows, Environmental impacts of tidal power schemes, in: Proceedings of the Institution of Civil Engineers-Maritime Engineering, Vol. 162, Thomas Telford Publishing, 2009, pp. 165–177.

[75] N. Yates, I. Walkington, R. Burrows, J. Wolf, Appraising the extractable tidal energy resource of the uk's western coastal waters, Phil. Trans. R. Soc. A 371 (1985) (2013) 20120181.

[76] H.E. Pelling, J.M. Green, Impact of flood defences and sea-level rise on the european shelf tidal regime, Cont. Shelf Res. 85 (2014) 96–105.

[77] A. Angeloudis, R. Falconer, Operation modelling of tidal energy lagoon proposals within the Bristol channel and Severn Estuary, in: Progress in Renewable Energies Offshore: Proceedings of the 2nd International Conference on Renewable Energies, 2016, pp. 503–512.

[78] D. Prandle, Simple theory for designing tidal power schemes, Adv. Water Resour. 7 (1) (1984) 21–27.

[79] M. Lewis, K. Horsburgh, P. Bates, R. Smith, Quantifying the uncertainty in future coastal flood risk estimates for the uk, J. Coast. Res. 27 (5) (2011) 870–881.

[80] M. Kadiri, R. Ahmadian, B. Bockelmann-Evans, W. Rauen, R. Falconer, A review of the potential water quality impacts of tidal renewable energy systems, Renew. Sustain. Energy Rev. 16 (1) (2012) 329–341.

[81] I. Fairley, R. Ahmadian, R.A. Falconer, M. Willis, I. Masters, The effects of a Severn Barrage on wave conditions in the Bristol Channel, Renew. Energy 68 (2014) 428–442.
[82] N. Čož, R. Ahmadian, R.A. Falconer, Implementation of a full momentum conservative approach in modelling flow through tidal structures, Water 11 (9) (2019) 1917.
[83] P. Jeffcoate, P. Stansby, D. Apsley, Flow and bed-shear magnification downstream of a barrage with swirl generated in ducts by stators and rotors, J. Hydraul. Eng. 143 (2) (2017) 06016023.
[84] A. Davies, P. Robins, Residual flow, bedforms and sediment transport in a tidal channel modelled with variable bed roughness, Geomorphology 295 (2017) 855–872.
[85] J. Xue, R. Ahmadian, R.A. Falconer, Optimising the operation of tidal range schemes, Energies 12 (15) (2019) 2870.
[86] J. Xue, R. Ahmadian, O. Jones, Genetic algorithm in tidal range schemes' optimisation, Energy 200 (2020) 117496.
[87] K. Pappas, L. Mackie, I. Zilakos, A.H. van der Weijde, A. Angeloudis, Sensitivity of tidal range assessments to harmonic constituents and analysis timeframe, Renew. Energy 205 (2023) 125–141.